Electronic Supplementary Material (ESI) for Dalton Transactions.
This journal is © The Royal Society of Chemistry 2016

*Supporting Information*

# Synthesis, structure, magnetic and biological activity studies of bis-hydrazone derived Cu(II) and Co(II) coordination compounds

**Upendarrao Golla,[a⊥] Amit Adhikary,[b⊥] Amit Kumar Mondal,[b] Raghuvir Singh Tomar[a]* and Sanjit Konar[b]***

[a]Department of Biological Science, IISER Bhopal, Bhopal 462066, M.P. INDIA. **Fax:** +91-755-4092392; Tel: +91-755-6692560; E-mail: rst@iiserb.ac.in

[b]Department of Chemistry, IISER Bhopal, Bhopal 462066, M.P. INDIA. **Fax:** +91-755-6692392; Tel: +91-755-6692339; E-mail: skonar@iiserb.ac.in

⊥Authors contributed equally

**Synthesis of ligand $H_2L^1$:** The ligand $H_2L^1$was synthesized by refluxing a solution of succinic dihydrazide (1.46 g, 10 mmol) and 2-pyridinecarboxaldehyde (2.14 g, 20 mmol) in 30 mL methanol for 12 h. The solution was cooled to room temperature and the solid precipitate obtained was filtered and washed with diethyl ether, dried in vacuum to give $H_2L^1$. Yield: 85 %. Elemental analysis calcd. (%) for $C_{16}H_{16}N_6O_2$ (bulk sample): C, 59.25; H, 4.97; N, 25.91. Found: C, 59.32; H, 5.02; N, 25.97.

**Synthesis of ligand $H_4L^2$:** The ligand $H_4L^2$ was synthesized by refluxing a solution of succinic dihydrazide (1.46 g, 10 mmol) and salicylaldehyde (2.44 g, 20 mmol) in 30 mL methanol for 12 h. The solution was cooled to room temperature and the solid precipitate obtained was filtered and washed with diethyl ether, dried in vacuum to give $H_4L^2$. Yield: 85 %. Elemental analysis calcd. (%) for $C_{18}H_{18}N_4O_4$ (bulk sample): C, 61.02; H, 5.12; N, 15.81. Found: C, 61.08; H, 5.17; N, 15.92.

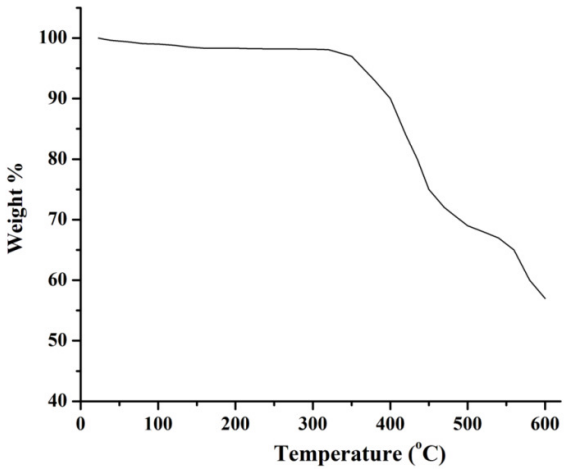


**Fig. S1:** Thermogravimetric (TG) analysis of compound **1**.

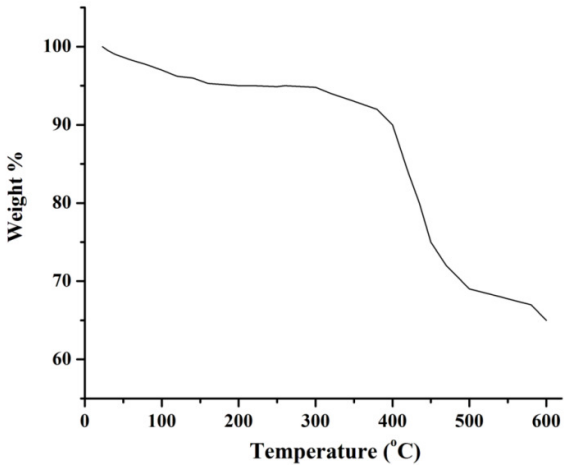


**Fig. S2:** Thermogravimetric (TG) analysis of compound **2**.

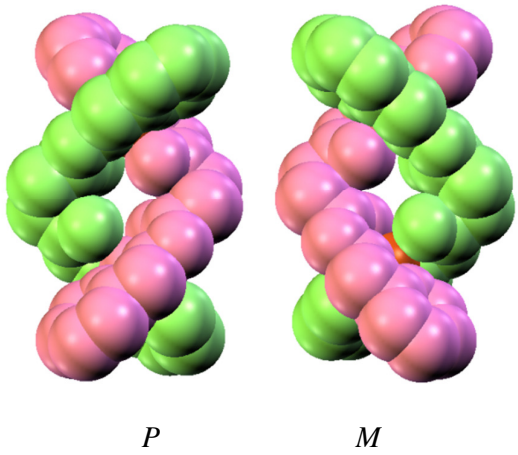


**Fig. S3:** Space-filling representations of the two independent cationic compounds $[Cu_2L^1{}_2]^+$ found in compound**1**with *P*- and *M*-helicity.

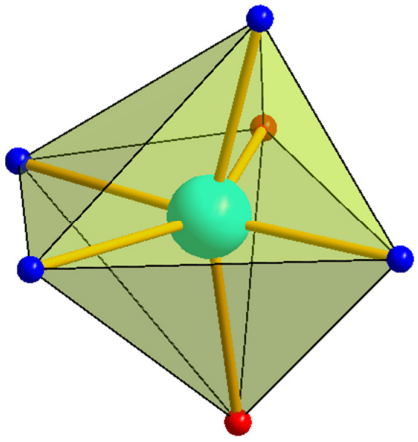

**Fig. S4:** A polyhedral view depicting distorted octahedral geometry around $Cu^{2+}$ with $N_4O_2$coordination in compound**1**.

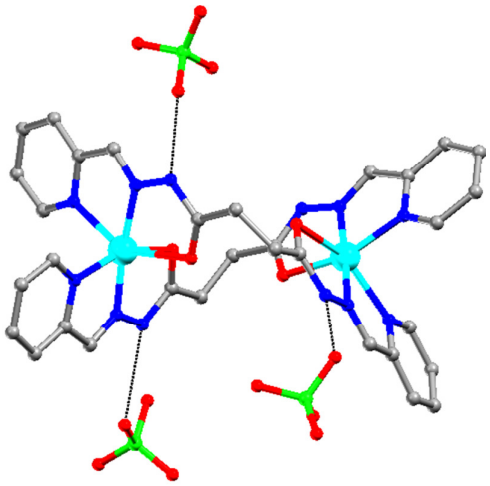

**Fig. S5:** H-bonding interactions between hydrazide-H and perchlorate anions of compound**1**.

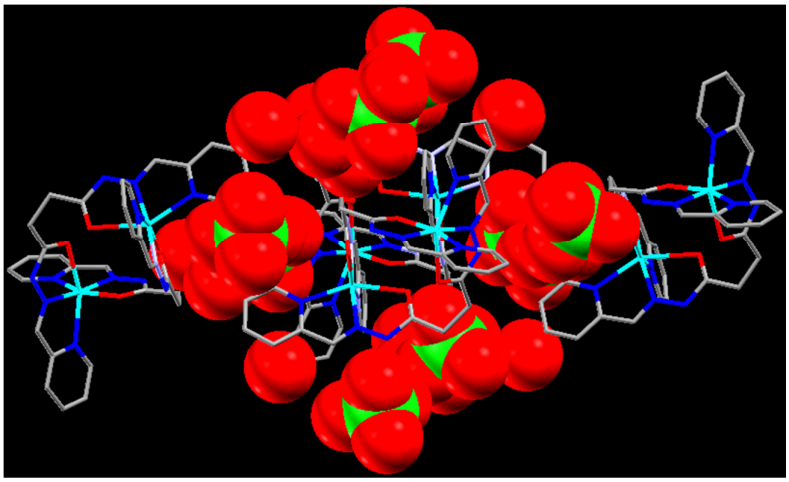

**Fig. S6:** A view of 1D arrangement of lattice solvents and anions through H-bonding interactions in the packing of compound**1**.

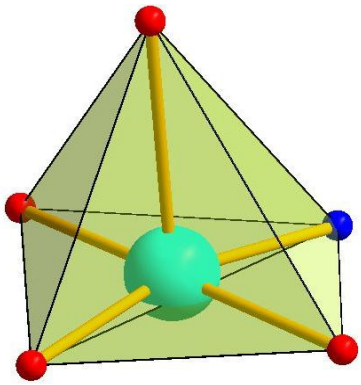

**Fig. S7:** A polyhedral view depicting distorted square-pyramidal geometry around $Cu^{2+}$ with $O_4N_1$ coordination in compound**2**.

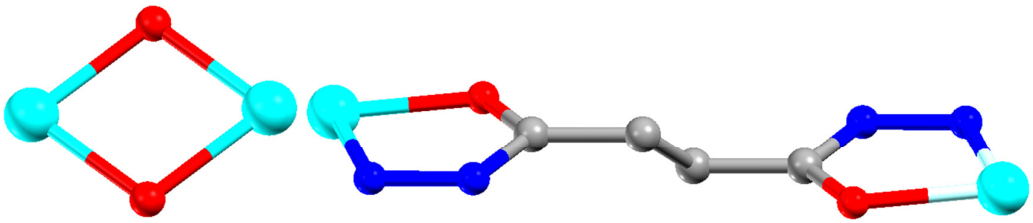

(a) (b)

**Fig. S8:** Two types ((a) and (b)) of bridging between two $Cu^{2+}$ in compound**2**.

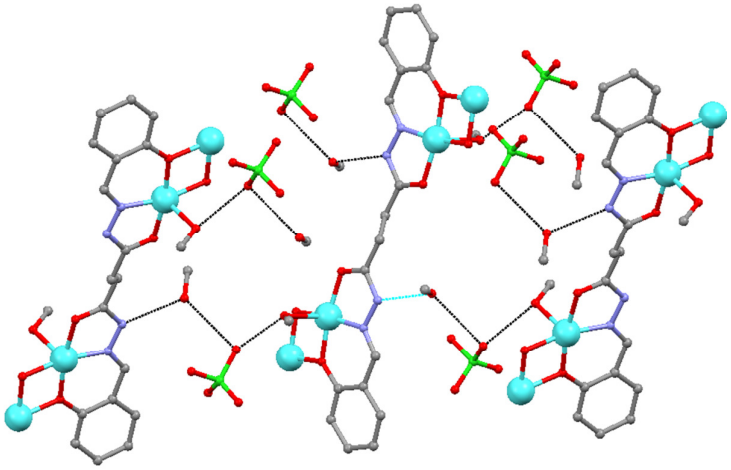

**Fig. S9:** H-bonding interactions between hydrazide-H and methoxy oxygen with solvent methanol andperchlorate anions of compound**2**.

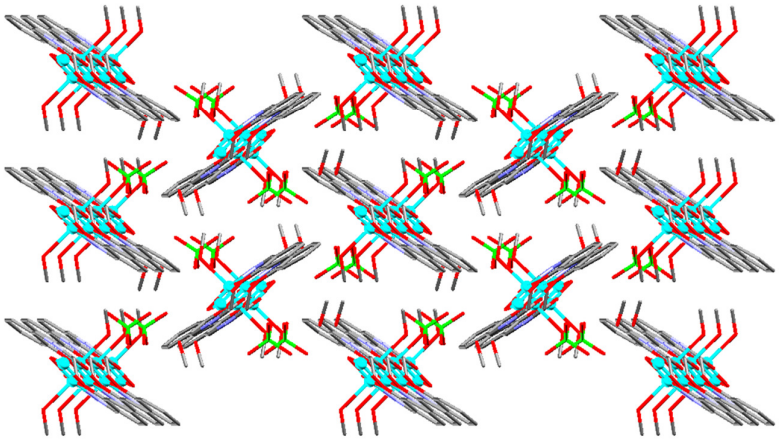

**Fig. S10:** Packing diagram of compound**2**.

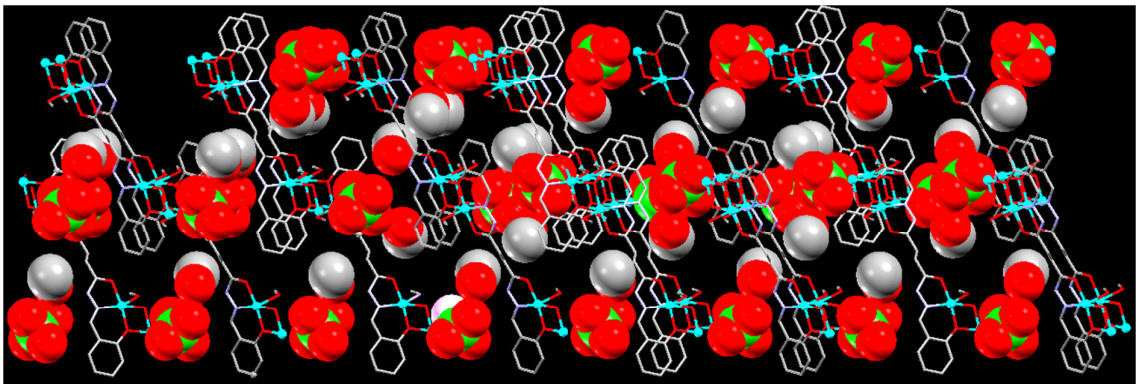

**Fig. S11:** A view of 1D arrangement of lattice solvents and anions in compound**2**.

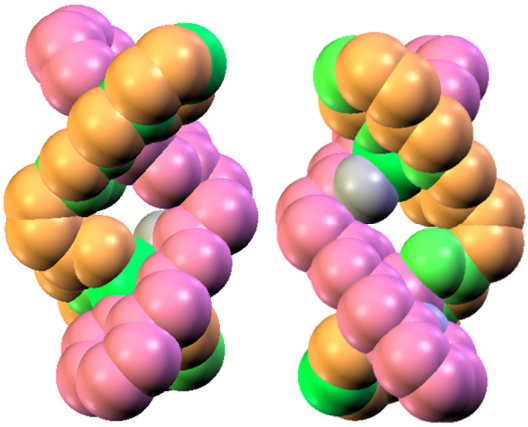

*PM*

**Fig. S12:** Space-filling representations of the two independent cationic compounds $[Co_2L^1{}_2]^{2+}$ found in compound**3**with *P*- and *M*-helicity.

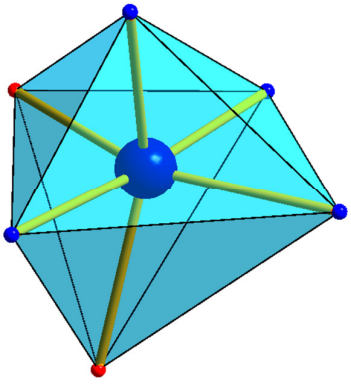

**Fig. S13:** A polyhedral view depicting distorted square-pyramidal geometry around $Co^{2+}$with $N_4O_2$coordination in compound**3**.

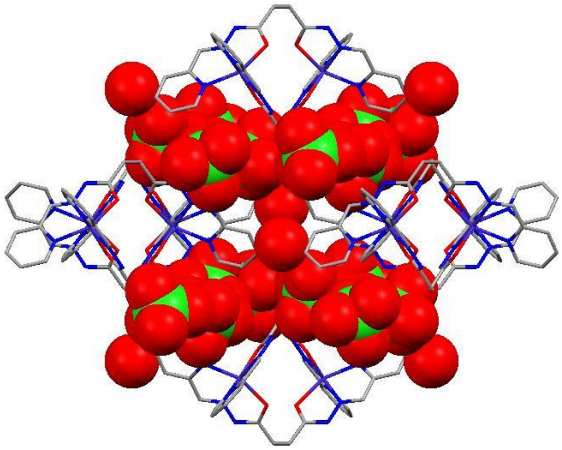

**Fig. S14:** A view of 1D arrangement of lattice solvents and anions through H-bonding interactions in compound**3**.

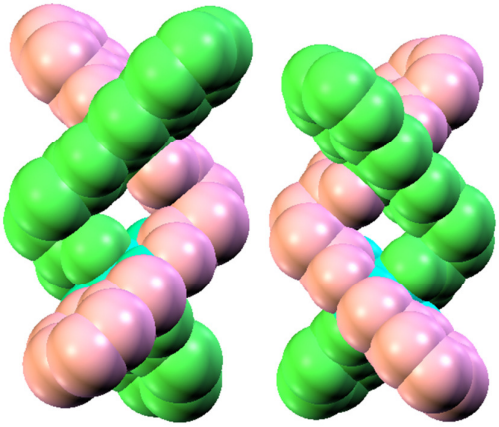

*PM*

**Fig. S15:** Space-filling representations of the two independent cationic compounds $[Co_2L^2{}_2]^{2+}$ found in compound**4**with *P*- and *M*-helicity.

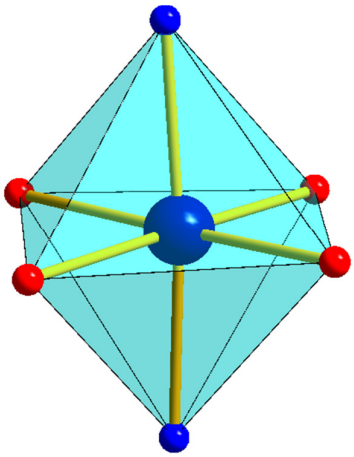

**Fig. S16:** A polyhedral view depicting distorted octahedral geometry around $Co^{2+}$ with $N_2O_4$coordination in compound**4**.

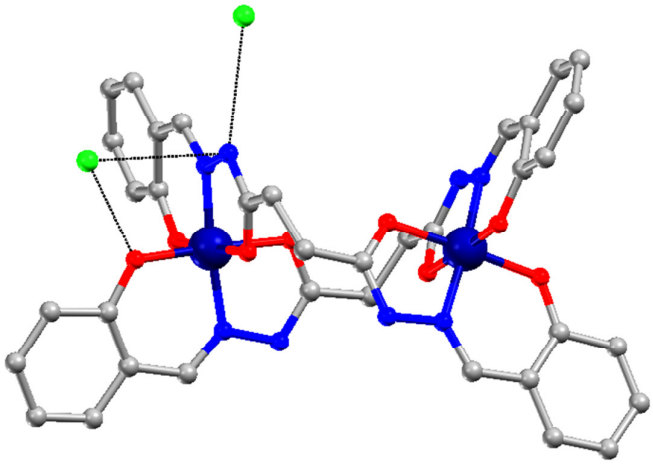

**Fig. S17:** H-bonding interactions between hydrazide-H and phenolic oxygen with chloride anions of compound**4**.

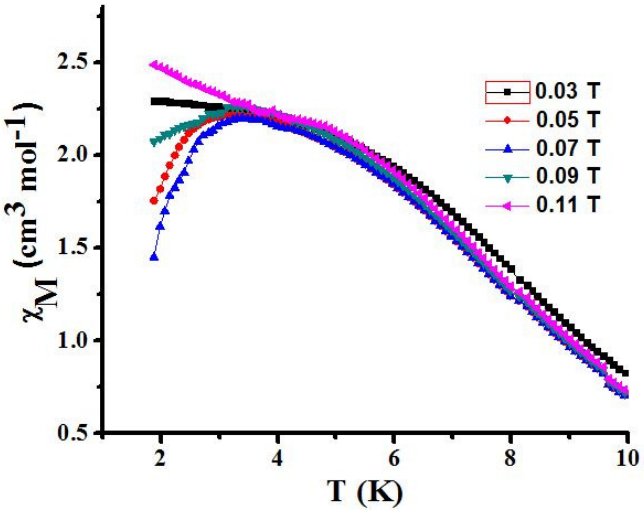


**Fig. S18:** Temperature dependence of magnetization of compound **3** at various dc fields.

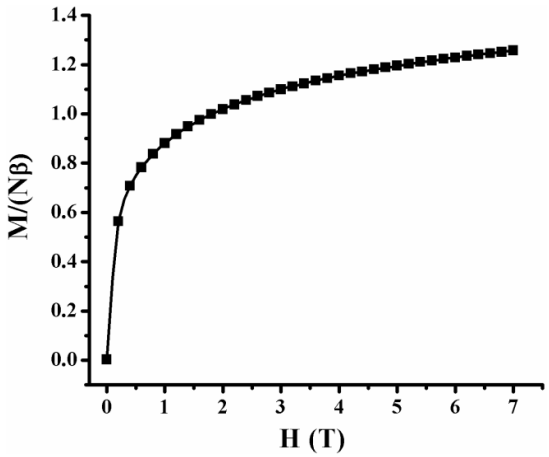


**Fig. S19:** Field-dependencies of isothermal normalized magnetizations of compound **3**, collected at 2 K.

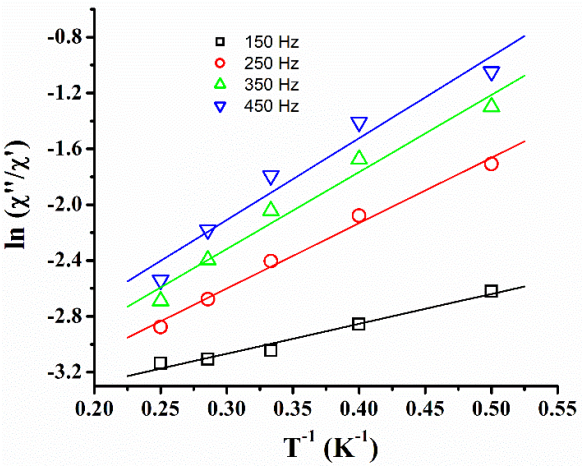


**Fig. S20:** Natural logarithm of the ratio of $\chi''$ over $\chi'$*vs.* 1/T for compound **3**. Solid lines indicate best fit obtained.

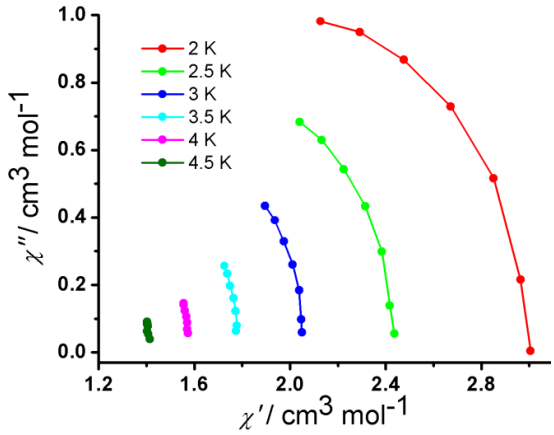


**Fig. S21:** Cole-Cole plot of compound **3**.

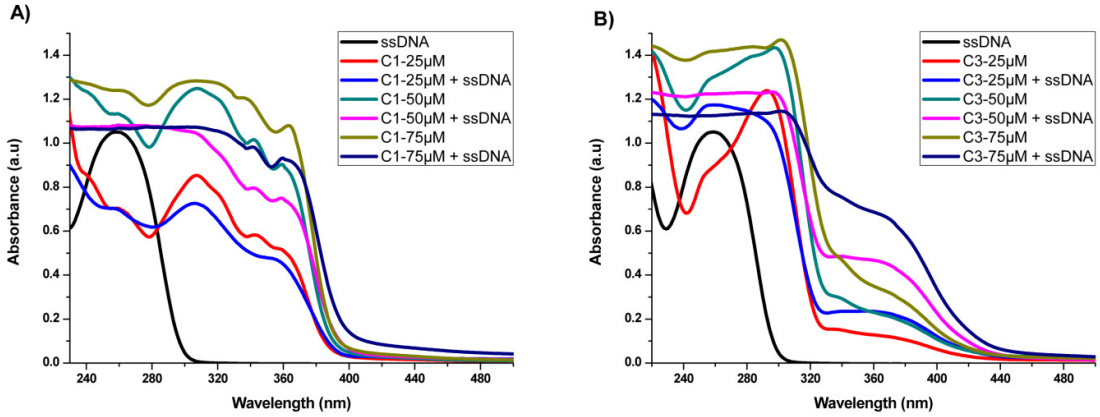


**Fig. S22:** UV-Visible absorption spectra of compounds 1 and 3 in the presence of SS-DNA. A & B) The compounds **1** (A) and **3** (B) of different concentrations (25, 50 and 75μM) were incubated with constant dose of SS-DNA (50μg/mL) for 2h at 37$^{o}$C. The absorption spectra of SS-DNA and compounds in alone or combination were obtained by using UV-Vis spectrophotometer.

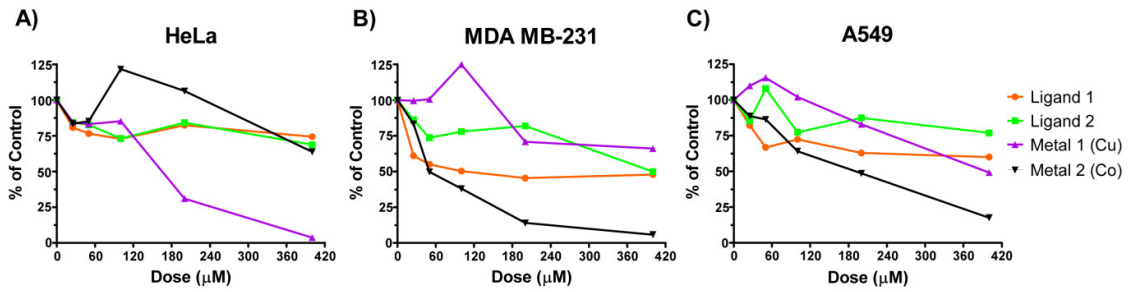


**Fig. S23:** The cytotoxic effect of ligands and metals on human tumor cell lines. A-C) The viability of human cervical cancer cells-HeLa (A), human breast adenocarcinoma cells-MDAMB-231 (B), and human lung carcinoma cells-A549 (C) treated with different doses of ligands (1, 2), and metals (1, 2) was measured by using typical MTT assay. The representative dose-response curves were plotted for each of cell lines and the % of viable cells was measured in comparison to untreated control.

**Table S1.** Bond Valence Sum (BVS) calculations for compound **1**.

| Cu site | BVS | Assigned oxidation state |
|---|---|---|
| Cu1 | 1.95 | 2 |
| Cu2 | 1.97 | 2 |

**Table S2.** Bond Valence Sum (BVS) calculations for compound **3**.

| Co site | BVS | Assigned oxidation state |
|---|---|---|
| Co1 | 1.98 | 2 |
| Co2 | 1.95 | 2 |